

# Lab on a Chip

Accepted Manuscript

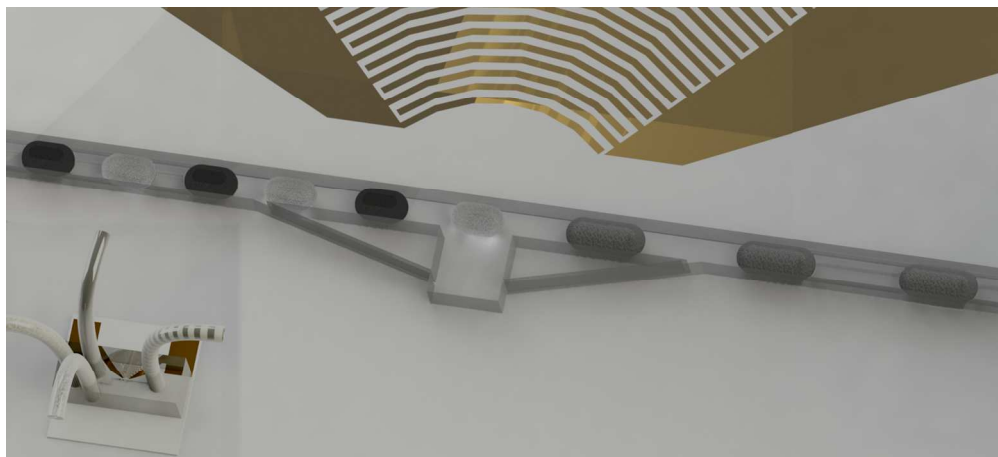


This is an *Accepted Manuscript*, which has been through the Royal Society of Chemistry peer review process and has been accepted for publication.

*Accepted Manuscripts* are published online shortly after acceptance, before technical editing, formatting and proof reading. Using this free service, authors can make their results available to the community, in citable form, before we publish the edited article. We will replace this *Accepted Manuscript* with the edited and formatted *Advance Article* as soon as it is available.

You can find more information about *Accepted Manuscripts* in the [Information for Authors](#).

Please note that technical editing may introduce minor changes to the text and/or graphics, which may alter content. The journal's standard [Terms & Conditions](#) and the [Ethical guidelines](#) still apply. In no event shall the Royal Society of Chemistry be held responsible for any errors or omissions in this *Accepted Manuscript* or any consequences arising from the use of any information it contains.



Digital microfluidic chip merges multiple consecutive droplets (nL) selectively and controllably using surface acoustic waves  
133x60mm (300 x 300 DPI)

# Microfluidic on-demand droplet merging using surface acoustic waves

†

Muhsincan Sesen,<sup>a</sup> Tuncay Alan,<sup>a</sup> and Adrian Neild<sup>\*a</sup>

Received Xth XXXXXXXXXXXX 20XX, Accepted Xth XXXXXXXXXXXX 20XX

First published on the web Xth XXXXXXXXXXXX 200X

DOI: 10.1039/b000000x

Individual droplets can be isolated within microfluidic systems by use of an immiscible carrier layer. This type of two phase systems, often termed “digital microfluidics”, find wide ranging applications in chemical synthesis and analysis. To conduct on-chip biochemical analysis, a key step is to be able to merge droplets selectively in order to initiate the required reactions. In this paper, a novel microfluidic chip integrating interdigital transducers is designed to merge multiple droplets on-demand. The approach uses surface acoustic wave induced acoustic radiation forces to immobilize droplets as they pass from a channel into a small expansion chamber, there they can be held until successive droplets arrive. Hence, no requirement is placed on the initial spacing between droplets. When the merged volume reaches a critical size, drag forces exerted by the flowing oil phase act to overcome the retaining acoustic radiation forces, causing the merged volume to exit the chamber. This will occur after a predetermined number of droplets have merged depending on the initial droplet size and selected actuation power.

## 1 Introduction

The field of microfluidics is driven by the vast possibilities offered by scaling down conventional benchtop laboratory processes and equipment. The miniaturization of analytical equipment into lab-on-a-chip (LOC) devices overcomes the limitations arising with bulky and expensive instrumentation through the reduction in sample and reagent volumes; resulting in lower analysis costs, shorter reaction times, higher resolution and sensitivity. Furthermore, batch-fabrication techniques provide low cost and disposable instruments ideal for point-of-care diagnostics and environmental sensors<sup>1</sup>.

One class of lab-on-a-chip (LOC) devices, termed digital microfluidics, isolate small droplets of sample fluids by use of an immiscible carrier fluid. In this way, these two phase systems can handle droplet assays whilst ensuring each sample is physically and chemically isolated. These droplets are typically created using hydrodynamic effects which occur when a flowing sample stream meets a flowing oil stream; the result is the production of a large number of monodisperse sample droplets interspaced by volumes of oil<sup>2–5</sup>.

Each droplet can be thought of as being analogous (at a much smaller scale) to a sample deposited in a test tube or the well of micro titre plate, in order to further the analogy, and enable on-chip biochemical assay, a series of additional

tasks need to be achievable at the chip scale, these include sorting<sup>6–10</sup>, merging<sup>10–14</sup>, splitting<sup>15–20</sup>, trapping<sup>21–26</sup>, dilution<sup>25,27</sup> and mixing<sup>28–31</sup>. It is essential to assure that such manipulation technologies are easy to integrate, robust, energy efficient and contamination free.

On-chip reaction of small chemical samples can be used for a number of applications, including the formation of particles, chemical synthesis, kinetics studies, biomolecule synthesis<sup>32</sup>, or for the study of fast organic reactions<sup>33</sup>. For the reactions to be initiated, the coalescence or merging of different droplets is required (e.g., samples and reagents). As such, the on-chip merging of specific sample droplets containing different chemicals, dilutions or volumes is a vital component for versatile LOC devices to enable biochemical assays. Two main methods for merging droplets have been explored to date, namely, electrocoalescence<sup>10–12</sup> and hydrodynamic methods<sup>13,14</sup>.

Electrocoalescence has been employed by researchers in order to facilitate merging of two adjacent droplets, it utilizes an electric field applied to high conductivity aqueous droplets immersed in a low conductivity continuous phase. Electrocoalescence method involves the charging of the droplets upon interaction with an electrical field; subsequent aggregation and coalescence then occur due to droplet-droplet interactions<sup>34</sup>. The applied electric field enhances contact between the dispersed aqueous droplets and enables droplet-droplet coalescence through the rupture of droplet-interface<sup>35</sup>. This requires the conductivity and permeability between two immiscible fluids to be different<sup>36,37</sup> and the droplets to be in close proximity.

† Electronic Supplementary Information (ESI) available: [details of any supplementary information available should be included here]. See DOI: 10.1039/b000000x/

<sup>a</sup>Department of Mechanical and Aerospace Engineering, Monash University, Clayton, VIC 3800, Australia. E-mail: [adrian.neild@monash.edu](mailto:adrian.neild@monash.edu); Tel: +61 3 990 54655

Hydrodynamic merging of droplets is achieved through clever microchannel geometry designs and requires no external actuation. Generally, a microfabricated speed bump is introduced further downstream to the formed train of droplets. When a droplet flows through the speed bump zone, its velocity decreases either due to designed physical restrictions<sup>13</sup> or due to an expansion in the channel<sup>14,38,39</sup>. The trailing droplet catches up and collides with the slowed droplet after which fusion takes place between the two droplets or more. However, the passive hydrodynamic techniques employed alone are not capable of merging droplets on-demand.

On-demand control is of significant importance for on-chip assays, where a range of reagents need to react with a range of samples (or sample dilutions). Thus, dealing with large numbers of identical droplets created by conventional hydrodynamic effects complicates this task. Recently, surface acoustic waves have been shown to be capable of producing single picolitre droplets on-demand<sup>40</sup>, in this work we demonstrate that the same actuation principle can be applied to merge multiple droplets on-demand; in this way, the easy integration of techniques becomes straightforward.

Ultrasonic waves offer, through non-linear effects, a range of forcing mechanisms which act on a different time scale to the ultrasonic oscillation. For instance, Bjerknes forces can draw particles to oscillating bubbles<sup>41</sup>, acoustic streaming is highly applicable to fluid mixing<sup>42,43</sup>, and acoustic radiation forces can be used to migrate<sup>44-46</sup> and collect<sup>47-50</sup> suspended particles, and to sort droplets<sup>9</sup>.

Surface acoustic waves (SAWs), a special type of ultrasonic wave propagating on the surface of a piezoelectric substrate, have been widely employed in microfluidic applications<sup>5,9,44,51-58</sup>. They offer a cost-effective fast response actuation source which is easy to fabricate and integrate, energy efficient, and safe to biological samples<sup>59</sup>. In this work, SAW generated acoustic radiation forces, arising due to the mismatch in the acoustic impedances (wave speed and density) of the oil and aqueous phases, will be used to stop the progress of a selected droplet, such that successive droplets will merge with the trapped droplet until a certain volume is reached; afterwards the merged droplet will be released from the acoustic trap. As the initial droplet is stationary prior to merging, there is no requirement placed on the spacing between the droplets.

## 2 Operating Principle

The system which has been developed for the purpose of merging droplets using SAW is depicted in Fig. 1. At the inlet, droplets are produced by use of T-junctions of continuous oil and water streams. Most of the experimental results presented here were gathered with two inlets (oil and water); the three inlet (oil, water and dye) design depicted was used to demonstrate merging of two droplets containing different

liquids. The channel along which the flow pushes the droplets measures 100  $\mu\text{m}$  wide by 50  $\mu\text{m}$  high, except at the expansion area where the channel width is 300  $\mu\text{m}$ . There are also two very thin channels which were originally intended to allow a bypass flow when the droplet is held at the expansion in fact, due to issues of feature resolution they were blocked and proved to be unnecessary for the successful operation of the system. Curved aluminum electrodes, deposited on a piezoelectric substrate, are arranged such that the center of curvature coincides with the expansion area in the channel; these electrodes are used to excite the SAW.

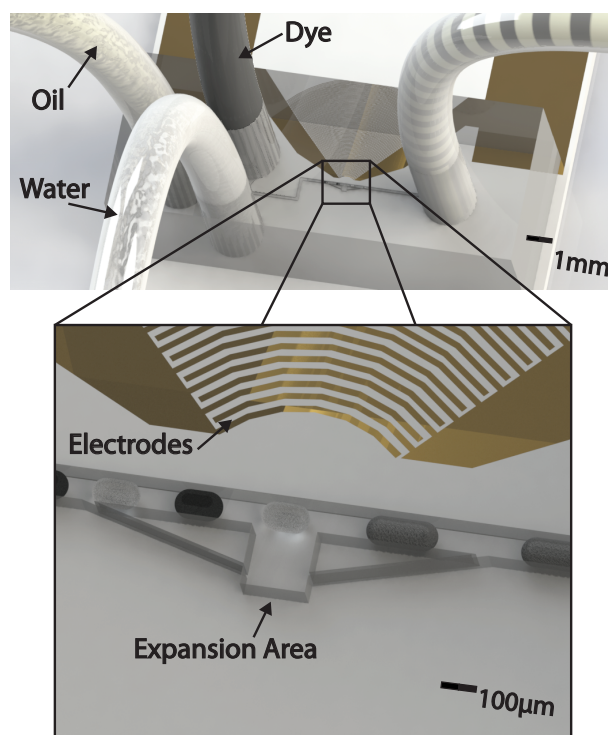


**Fig. 1** Microfluidic droplet merging chip design. Water and dye streams are designed to form T-junctions with the oil flow so that alternating droplets are generated. Droplets are trapped right across the electrodes due to surface acoustic waves so that the upcoming droplet can come and merge with the stopped one.

SAWs are acoustic waves with nm-scale amplitudes, oscillating in the MHz range and propagating along the surface of a piezoelectric substrate. Direct piezoelectric surface wave transduction was first introduced in the microscale<sup>60</sup> by use of inter-digital transducers (IDTs), such as those used here, consisting of periodic electrodes on a piezoelectric substrate. When an oscillating electrical signal of suitable frequency is applied to the IDTs, constructive interference between the waves generated at each electrode occurs. The required resonant frequency,  $f$ , is dictated by the pitch of the electrodes which is equal to half the wavelength,  $\lambda/2$ , accord-

ing to  $f = c_s/\lambda$ , where  $c_s$  is the sound speed on the substrate surface.

As the thickness of the substrate ( $500\ \mu\text{m}$ ) is chosen to be much larger than the wavelength, the resultant waves can be classified as Rayleigh waves<sup>61</sup>; these are energy efficient since the majority of the acoustic energy travels along the surface without dissipating into the depth of the solid by more than a few wavelengths. In addition by use of curved IDTs the waves can be easily focused on the substrate, in our case they are focused at the location of the channel expansion.

When the surface acoustic waves traveling along the piezoelectric substrate with a (Rayleigh) sound speed of  $c_s$  comes into contact with the fluid medium with a sound speed of  $c_l$ , acoustic energy is coupled to the liquid. The resulting wave in the fluid propagates at the Rayleigh angle found by  $\theta_R = \sin^{-1}(c_l/c_s)$  - depicted in Fig. 2(a). The focused nature of the waves on the substrate will give rise to spatial variations in the intensity of the coupled pressure waves. It is these pressure waves in the fluid which will be used to merge the droplets.

In many cases the calculations of the force field which acts on inhomogeneities in the fluid leads simply from knowledge of the pressure field. In the case of a one-dimensional field, for example, expressions are available for both a traveling and standing wave scenario, and some of the expressions are valid for inhomogeneities larger than the wavelength of the pressure field<sup>62</sup>. In the case of more complex sound fields, the equation provided by Gorkov<sup>63</sup> is widely applied. However this is limited to particles significantly smaller than the wavelength. In this work, the wavelength of the sound waves excited in the continuous medium is  $28.86\ \mu\text{m}$  and the droplets vary between  $100\ \mu\text{m}$  and  $150\ \mu\text{m}$  in diameter, furthermore the field is not one-dimensional, consisting instead of a focused series of substrate waves coupling at a given angle into the fluid. As such no analytical solution is available to move from pressure field to force field. Recently, it was shown that when particles of diameter,  $d$ , are subjected to SAW with wavelength,  $\lambda$ , while  $\lambda \approx d$ , a net acoustic force is induced on the particles due to acoustic scattering<sup>64</sup>.

An analogy can be drawn between a focused acoustic field and that of a focused optical beam, such an analogy has been used by Lee and Shung, with the acoustic beam being generated by an axially focused transducer<sup>65</sup> (Fig. 2(b)). In a single beam optical trap two forces are generated on a particle with different optical properties to those of the suspension medium, they are scattering induced forces and gradient forces<sup>66</sup>. The scattering forces tend to push particles in the direction of the optical propagation, whilst the gradient forces, which arise from spatial intensity variations due to focusing, tend to move particles towards high intensity zones. Hence, one breakthrough in optical trapping was the demonstration that a single optical beam can trap a particle<sup>67</sup>, provided that

it is focused, as in this case the gradient forces dominate over the scattering forces (Fig. 2(b)).

A clear and significant shortcoming in this analogy arises when it is considered for a focused SAW beam due to the different wave propagation direction. In an axially focused beam (optical or acoustic) the propagation direction is through the waist of the beam, whilst in the case of the focused SAW beam, the focusing is along x-direction (Fig. 2(c)) and propagation is in the y-z plane (Fig. 2(a)). What this means is that the scattering forces due to propagation direction, can be expected to be at an angle to the focal plane, due to the additional constraint of the droplet being encapsulated in a channel, the scattering forces will simply push the droplet against the roof of the channel, thus we would expect the gradient forces to dictate droplet movement in the x-y plane. Time averaged surface displacement on the lithium niobate substrate shown in Fig. 2(c) was captured using a Laser Doppler Vibrometer, there is a clear intensity variation along the channel, peaking at the location of the expansion chamber.

The droplets used in this work are in the Mie regime where the droplet diameter,  $D$ , is of similar magnitude to the wavelength,  $\lambda$  (i.e.  $\lambda \approx D$ ). Geometrical (ray) acoustics, where sound is modeled as rays, can be used for modeling acoustic/optical trapping in the Mie regime<sup>68</sup>. In such a case, droplets are attracted towards high intensity ultrasound zones<sup>69</sup>.

The other key force acting on the droplet in the trapping region is that of drag. In its simplest form, i.e. when considering a particle in an infinite volume of fluid, Stokes drag is given by

$$F_d = 6\pi\mu r v \quad (1)$$

where  $\mu$  is the viscosity of the continuous fluid,  $r$  is the radius of the droplet and  $v$  is the velocity of the flow; provided that the acoustic force is sufficient to overcome this force, the droplet will remain trapped.

### 3 Fabrication

The IDTs used in this study were  $80\ \mu\text{m}$  wavelength (45.8 MHz) focused IDTs composed of 45 finger-pairs, the arc subtends an angle of  $90^\circ$ . Focused IDTs (FIDTs) are a special type of IDTs where finger pairs are formed into concentric circular arcs rather than the conventional straight finger pairs. This was first proposed by Green et al.<sup>72</sup> and employed in a number of recent studies<sup>40,47,73</sup>.

A 200nm thick aluminum layer of FIDT features were deposited onto 0.5 mm thick, double side polished  $128^\circ\text{Y}$ -cut, X-propagating lithium niobate,  $\text{LiNbO}_3$ , substrate. The silicon master mold for the designed microfluidic channels was fabricated using standard lithography and dry etching techniques

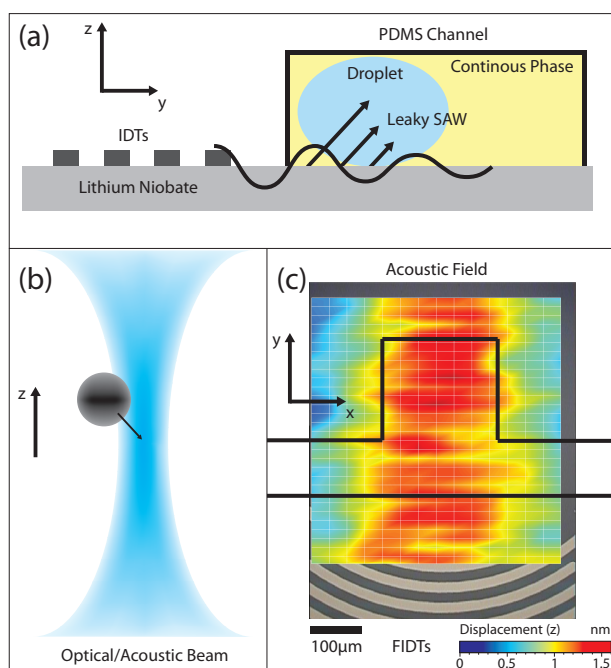


**Fig. 2** (a) Leaky SAWs travel on the piezoelectric substrate surface and exponentially decay as they leak into the fluid medium. (b) Optical/acoustic beam lying on  $z$ -axis have been shown to attract droplets in the Mie regime towards the focus point where the intensity is maximum<sup>70,71</sup>. (c) The time averaged out-of-plane ( $z$ ) surface displacement on the lithium niobate substrate captured using a Laser Doppler Vibrometer (LDV) shows that the acoustic field in the  $x$ - $y$  plane is focused along the  $x$ -direction in the area of the expansion chamber.

(50  $\mu\text{m}$  deep). The patterns were transferred to polydimethylsiloxane (PDMS) (SYLGARD<sup>®</sup> 184, Dow Corning) (10:1) using the master mold and individual devices were bonded to the diced lithium niobate devices after exposure to an activated air plasma (Harrick Plasma PDC-32G).

## 4 Experimental

The tubing for the inlets and outlets were connected to the device and syringes. The syringes were operated by two or three (depending on the number of inlets) NE-1000 (New Era Pump Systems, Inc.) syringe pumps to get the desired flow rates into the microfluidic channel network. The device was stabilized on a 3D-printed platform housing a peltier cooler and a fan. The entire setup was placed on the stage of a microscope (Olympus BX43, Tokyo, Japan) and videos were captured using a 5MP eyepiece camera (Dino-Lite AM7023B, New Taipei City, Taiwan). Oil was used as the continuous phase (viscosity,  $\mu = 85\text{cP}$ , surface tension at oil-water interface,  $\sigma_{w/o} \approx 0.024\text{N/m}^{74}$ ), whereas the dispersed phase was DI-water.

SAWs were generated by applying an AC signal across the electrode pads using a SMC100A signal generator (Rohde&Schwarz) amplified by AR 25A250A amplifier (Amplifier Research). The reported power values are measured using a WaveSurfer 454 oscilloscope (Teledyne LeCroy). The operating frequency of each device was determined using Power Signal Generator - F20 (BelektronikG, Bruenig & Guhr Elektronik GbR) by minimizing the reflected power from each device over a range of frequencies. Lithium niobate surface displacement was measured and visualized using a laser Doppler vibrometer (Polytech GmbH UHF-120, Waldbronn, Germany).

## 5 Results

As a droplet enters the channel expansion it will slow due to hydrodynamic effects but will not come to rest. The velocity of droplets passing through the expansion chamber, under no SAW actuation, is shown for a range of flow rates in Fig. 3(a). Droplet velocities were calculated by measuring the number of pixels traveled by the droplets during the time between each successive frame and a smoothing function (3-point moving average) was applied to the results with MATLAB software. In Fig. 3(b), the progress of a single droplet can be seen from a composite image which consists of seven superimposed frames (equally spaced in time).

In contrast, Fig. 4 shows, by way of a time series of images, the progress of a droplet under the influence of an acoustic field excited by SAW. It can be seen that the droplet comes to a complete stop at the center line of the focused IDTs (Fig.

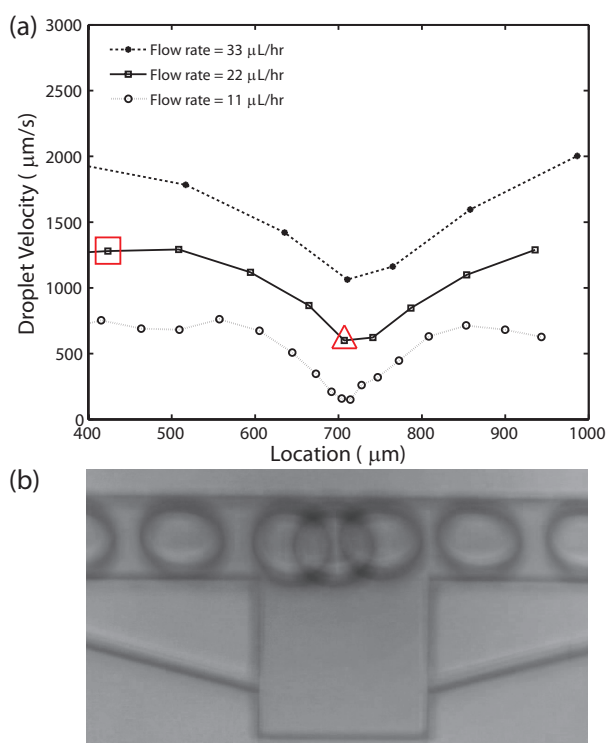


**Fig. 3** (a) In-channel droplet velocity profiles for different flow rates. Droplet velocities are calculated along the area of interest and a smoothing function (3-point moving average) was applied using MATLAB software. (b) 7 frames (equally spaced in time) have been superimposed to show the progress of the droplet through the expansion chamber. (The red square and triangle are referred to in the caption for Fig. 5)

4,  $t=1.2$ s). After the droplet was rendered immobile, the oil phase was able to flow around the droplet through the expansion area (Fig. 4,  $t=2.2$ s). Subsequently a second droplet enters the expansion chamber and merges with the first (Fig. 4,  $t=2.6$ s), the resultant larger droplet then moves out of the acoustic trap (Fig. 4,  $t=2.8$ s).

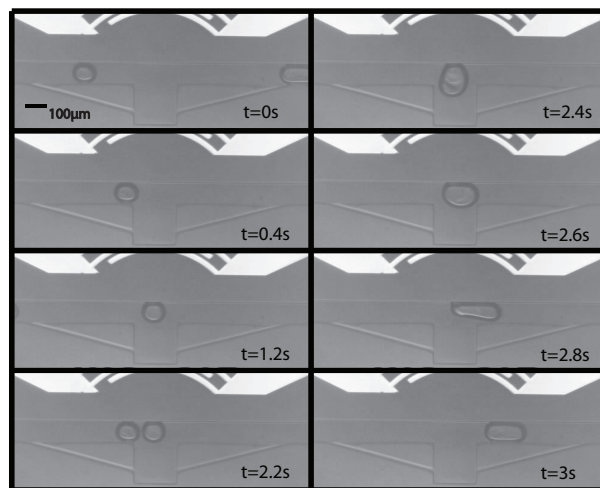


**Fig. 4** Time lapse images of the droplet merging experiment. The first droplet is immobilized across the FIDTs while the next droplet comes and merges with the stationary one. The merged droplet travels downstream because the acoustic energy in the system is not enough to hold a bigger volume droplet. The oil flow is from left to right.

Having demonstrated the principle of SAW droplet trapping and merging, we now examine the operational conditions required to achieve this. The minimum trapping power required to merge droplets of different velocities was analyzed by conducting a series of experiments in which the power was slowly increased until a droplet in varying fluid flow rates was trapped (Fig. 5). The flow rates applied to the two inlets were increased uniformly, resulting in droplets of equal sizes being formed. The data is plotted in two ways, in that the power is plotted against two sets of droplet velocities; firstly, the square data points use the droplet velocity in the channels before the expansion easily extracted from Fig. 3 (the maximum velocity values). However, it is known from Fig. 3 that the droplets slow due to hydrodynamic effects as they pass through the expansion even when unimpeded by acoustic effects. The second set of droplet velocities are for the velocity at which a droplet travels through the expansion in the absence of ultrasonic effects (i.e. the minimum value in the plots shown in Fig. 3). When halting a droplet ultrasonically, the drag force needs to be exceeded by the ultrasonic force. The location at which the droplets are halted is inside the expansion area, hence it is drag related to this velocity which needs to be overcome. It can be seen from this second set of data that there is

an almost linear relationship between droplet velocity inside the expansion and required acoustic power for the first three data points ( $< 22 \mu\text{L/hr}$ ) (asterisks in Fig. 5). We believe that the linearity is lost at higher flow rates and higher amplitudes due to experimental difficulties.

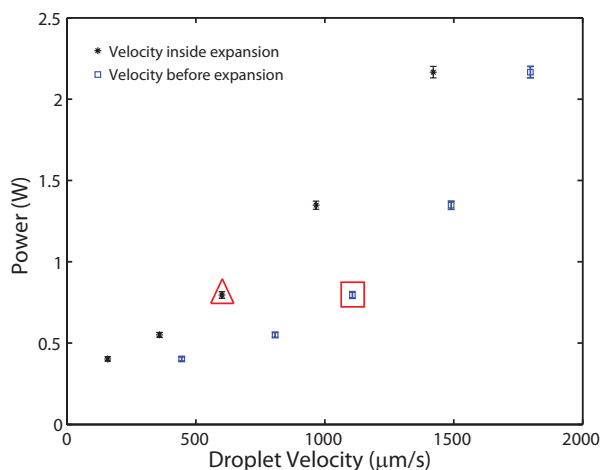


**Fig. 5** Minimum trapping power for droplets of  $0.447 \pm 0.013$  nL volume generated at increasing flow rates. Maximum and minimum droplet velocities were calculated and averaged before and inside the expansion area, respectively, while acoustic energy was not present (Fig. 3). The data point highlighted with the red triangle and square use the velocity data points in Fig. 3 which are highlighted the same way.

In order to understand this outcome, it is worth considering the relationship between parameters affecting the forces concerned:

$$P_i \propto \xi^2 \propto p^2 \propto F \quad (2)$$

It has previously been shown that power input,  $P_i$ , is proportional to piezoelectric surface velocity squared<sup>75</sup>,  $\xi^2$ . This surface vibration velocity relates directly to pressure amplitude,  $p$ , generated in the liquid medium<sup>76</sup>. Acoustic radiation force,  $F$ , is proportional to pressure amplitude squared<sup>63</sup>,  $p^2$ . This force is used to balance (at its lower limit) or overcome Stokes' drag which depends on flow velocity,  $v$ , linearly (Eqn. 1). Overall, then, it must be expected that the minimum required power input to the system be linearly related to the droplet velocity.

The flow rates at the oil and water inlets were altered over a series of experiments to investigate the relationship between minimum required power for droplet trapping and droplet volume. The alteration of these flow rates causes droplets of different sizes to be created<sup>77</sup>, though, clearly it also alters the flow rate against which the droplet must be retained. This latter effect is governed by the combined flow rate at the inlets,

which was varied between 6 and 11  $\mu\text{L/hr}$ . Since flow rate is also a function of minimum trapping power; a linear approximating function derived for droplet velocity inside the expansion and minimum trapping power (extracted from the data shown in Fig. 5) was used to scale the experimental power values matching a flow rate 8  $\mu\text{L/hr}$  where applicable.

The minimum trapping power for various droplet volumes is displayed in Fig. 6(a). It can be seen (with reference to the data points shown as asterisks) that the trapping of larger droplets requires larger input powers, this means that when operating at these critical power levels, a droplet can be held, but when a second droplet comes into the channel and merges with the first, the resultant volume rise will ensure that the power is not sufficient to trap the combined volume, hence the droplet will move out of the expansion. The trap, merge and release sequence shown in Fig. 4 is thus assured at these powers.

The droplet volumes were calculated through image processing, for each data point taking into account a minimum of three images and averaged, the standard deviations are used for the error bars. The droplet volumes plotted are calculated before merging occurred, i.e. considering the volume of a single droplet in the trapping area.

For increasing droplet volume, the expansion chamber becomes increasingly blocked, leaving a smaller space for the oil to flow past. The trapped droplet therefore experiences more drag force exerted by the continuous phase flow. When the droplet volume is further increased, the entire channel will become blocked and the current setup is unable to trap the droplet because there's insufficient space for the continuous phase to flow (see Fig. 6(b)). The presence of the trapped droplet in such a confined space means that Stokes drag which predicts linearity between radius and drag, no longer applies.

Haberman and Sayle<sup>78</sup> presented an analytical drag formula to calculate the drag force,  $F_{d,conf}$  on a stationary sphere of radius  $r$  confined in a circular pipe of radius  $a$ . It is given, as a function of Stokes drag, by:

$$F_{d,conf} = \frac{(1 - \frac{2}{3}R^2 - 0.20217R^5)F_d}{1 - 2.105R + 2.0865R^3 - 1.7068R^5 + 0.72603R^6} \quad (3)$$

where  $R$  is the ratio of the confinement radii,  $R = r/a$ , and  $F_d$  is the unconfined drag on the particle - the Stokes' drag. Whilst this scenario is not exactly that of the system under examination here, it gives a better understanding of the drag acting on an object in an increasingly blocked channel.

In Fig. 6(a), this drag force (predicted to be scaling linearly with trapping power in Eqn. 2) was normalized, scaled and plotted for experimental droplet volume values with matching  $a$  and  $r$  values gathered from the experiments as shown in Fig. 6(c). Again it is worth emphasizing that we cannot expect a highly accurate agreement against our data, as the droplets are

trapped in a syringe driven rectangular cross-section flow as opposed to pressure driven axi-symmetric flow. However, a sharp increase in the analytical drag force can be observed as the flow is further restricted by increasing droplet size, which is of a similar nature to the increase in power required to trap the droplets. Stokes' drag by itself cannot account for confined flow which is why the minimum power needed to trap droplets of bigger volume grows asymptotically in the experimental results as well.

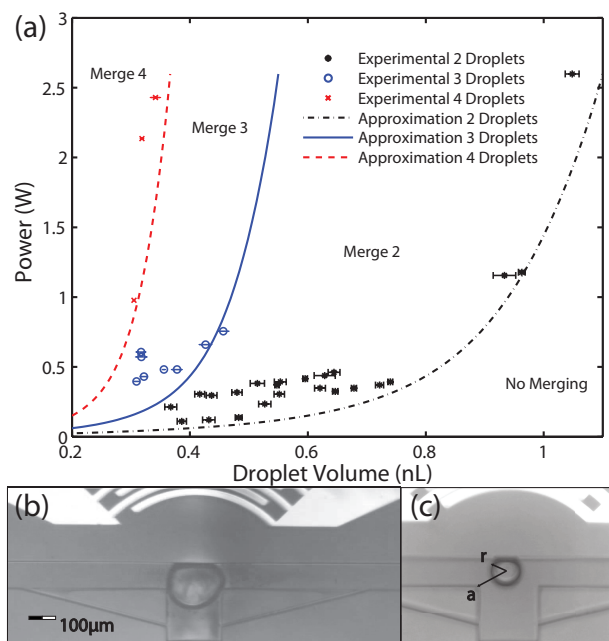


**Fig. 6** (a) Minimum required trapping power as a function of droplet volume. Droplet size measurements were carried out through image processing considering a minimum of three images and averaged, standard deviations are shown as error bars. The graph is labeled to show regions where merging will not occur, as well as regions in which 2,3, and 4 droplets will merge. Data for two droplets merging is shown in asterisks (black). The solid line (black) shows the analytically found drag force on the droplet in a constricted flow. To consider the merging of multiple droplets, the drag is scaled in the x direction, such that, for example for four droplet merging, the critical drag which must be overcome is that of 3 times the initial droplet volume. To support this, a data point for the merging of both three (blue) and four (red) droplets is shown. (b) A 1.08 nL volume droplet that the current setup was unable to trap with maximum acoustic energy. It can be seen that the expansion chamber is completely filled by the droplet and there is no space for the continuous phase to flow. Haberman and Sayle's analytical drag formula<sup>78</sup> for a stationary sphere of radius  $r$  confined in a circular pipe of radius  $a$  ( $a \gg r$  calculated from experimental data as shown in (c)) was scaled and plotted as approximations for merging 2,3, and 4 consecutive droplets.

There is also the possibility of using excessive power to trap

the first droplet. This can lead to the merging of more than two droplets. This system has been used for the merging of up to 4 consecutive droplets. Experimental results for merging of 3 and 4 consecutive droplets are also shown in Fig. 6(a). Time-lapse images for merging three droplets is shown in Fig. 7.

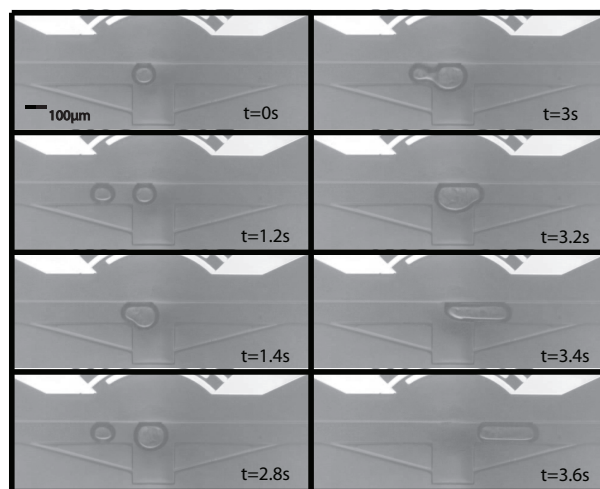


**Fig. 7** Experimental results showing time lapse images of the 3-droplet merging experiment. The first droplet (0.4452 nL) is immobilized across the IDTs while the next droplet comes and merges with the stationary one ( $t=1.4s$ ). The first two droplets stay trapped until the third droplet comes and merges with the lot ( $t=3s$ ). As droplet volume is tripled, the system is unable to trap the droplet anymore therefore it is released from the trapping zone ( $t=3.4s$ ).

The power required to perform this multiple droplet merging is shown in Fig. 6(a) with a circle (blue) and a cross (red) data point, for 3 and 4 droplets respectively. Approximating functions for merging of 3 and 4 droplets are calculated by scaling down (x-axis) the original 2 droplet approximation curve by a factor of 2 and 3 respectively. Reported droplet volumes are for the first droplet only, however, the minimum trapping power is for trapping  $n - 1$  droplets where  $n$  is the total number of droplets merged (i.e 3 droplets are trapped for merging 4 droplets). This is why scaling down the approximation curve is straightforward; this way, regions of droplet volume and input power combinations emerge, in which no trapping occurs, or the merging of 2,3 or 4 droplets can be expected (Fig. 6(a)).

Finally, in order to demonstrate a possible application for the designed microfluidic chip, droplets of water and black dye were merged on demand. Time-lapse images of the experiment are shown in Fig. 8. Alternating droplets were achieved by use of 2 different T-junctions which joined oil, water and dye inlets, prior to the merging chamber (Fig. 1). The merging of these pure water and dye droplets, represents how samples and reagent droplets, for example, could readily be merged on demand, offering reduced reaction times and quantities of

fluids used.

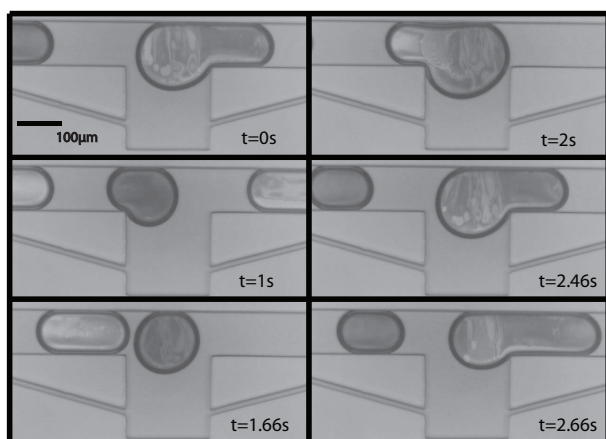


**Fig. 8** Experimental results showing time lapse images of the droplet merging experiment with alternating droplets of water and black dye.

It should be noted that the volume of the smallest droplets trapped was limited to 0.3 nL (94.07 µm dia.) by the design of droplet generating T-junctions. Whilst, the maximum volume of droplets which could be trapped, 1.1 nL (167.36 µm dia.), was limited by constriction effects, and hence the geometry of the expansion chamber. The number of droplets trapped prior to release is dictated by a combination of the chamber geometry and the power used to excite the acoustic waves. Hence, it is reasonable to expect that it is possible to merge droplets of bigger or lesser volume by suitable designing of the expansion chamber, T-junction and FIDTs.

The throughput of the system was not optimized, however, it is worth noting that 2 droplets could be merged every 0.3 seconds, most of the time being spent in waiting for the second droplet to arrive. Future work includes improving the throughput of the system by increasing flow rates and optimizing the expansion chamber design.

## 6 Conclusions

It was experimentally shown that multiple droplets can readily be trapped and merged on demand using surface acoustic waves (SAWs). The minimum required trapping power for similar size droplets in varying flow rates were established with experimental results. Experimental results for the minimum trapping power as a function of droplet volume ranging from 0.3 to 1 nL were discussed for merging up to four consecutive droplets. To demonstrate a potential application, alternating water and black dye droplets were successfully merged on demand using the proposed microfluidic chip. SAW based droplet merging have the potential to replace existing technologies and serve as the next generation droplet merging

technique because it offers power consumption, seamless integration and contamination free on-demand operation independent of droplet spacing.

## 7 Acknowledgements

This work was performed in part at the Melbourne Centre for Nanofabrication (MCN) in the Victorian Node of the Australian National Fabrication Facility (ANFF).

## References

- 1 D. C. Duffy, J. C. McDonald, O. J. A. Schueller and G. M. Whitesides, *Analytical Chemistry*, 1998, **70**, 4974–4984.
- 2 T. Thorsen, F. H. Roberts, F. H. Arnold and S. R. Quake, *Physical Review Letters*, 2001, **86**, 4163–4166.
- 3 S. L. Anna, N. Bontoux and H. A. Stone, *Applied Physics Letters*, 2003, **82**, 364–366.
- 4 C. Cramer, P. Fischer and E. J. Windhab, *Chemical Engineering Science*, 2004, **59**, 3045–3058.
- 5 L. Schmid and T. Franke, *Lab Chip*, 2013, **13**, 1691–1694.
- 6 J. J. Agresti, E. Antipov, A. R. Abate, K. Ahn, A. C. Rowat, J.-C. Baret, M. Marquez, A. M. Klibanov, A. D. Griffiths and D. A. Weitz, *Proceedings of the National Academy of Sciences*, 2010, **107**, 4004–4009.
- 7 K. Ahn, C. Kerbage, T. P. Hunt, R. M. Westervelt, D. R. Link and D. A. Weitz, *Applied Physics Letters*, 2006, **88**, 024104–024104-3.
- 8 J.-C. Baret, O. J. Miller, V. Taly, M. Ryckelynck, A. El-Harrak, L. Frenz, C. Rick, M. L. Samuels, J. B. Hutchison, J. J. Agresti, D. R. Link, D. A. Weitz and A. D. Griffiths, *Lab Chip*, 2009, **9**, 1850–1858.
- 9 T. Franke, A. R. Abate, D. A. Weitz and A. Wixforth, *Lab Chip*, 2009, **9**, 2625–2627.
- 10 D. R. Link, E. Grasland-Mongrain, A. Duri, F. Sarrazin, Z. Cheng, G. Cristobal, M. Marquez and D. A. Weitz, *Angewandte Chemie International Edition*, 2006, **45**, 2556–2560.
- 11 K. Ahn, J. Agresti, H. Chong, M. Marquez and D. A. Weitz, *Applied Physics Letters*, 2006, **88**, 264105–264105-3.
- 12 C. Priest, S. Herminghaus and R. Seemann, *Applied Physics Letters*, 2006, **89**, 134101–134101.
- 13 X. Niu, S. Gulati, J. Edel *et al.*, *Lab Chip*, 2008, **8**, 1837–1841.
- 14 N. Bremond, A. R. Thiam and J. Bibette, *Phys. Rev. Lett.*, 2008, **100**, 024501.
- 15 T. S. Kaminski, S. Jakiela, M. A. Czekalska, W. Postek and P. Garstecki, *Lab Chip*, 2012, **12**, 3995–4002.
- 16 F. Scheiff, M. Mendorf, D. Agar, N. Reis and M. Mackley, *Lab Chip*, 2011, **11**, 1022–1029.
- 17 D. N. Adamson, D. Mustafi, J. X. J. Zhang, B. Zheng and R. F. Ismagilov, *Lab Chip*, 2006, **6**, 1178–1186.
- 18 D. R. Link, S. L. Anna, D. A. Weitz and H. A. Stone, *Phys. Rev. Lett.*, 2004, **92**, 054503.
- 19 A. C. Hatch, J. S. Fisher, A. R. Tovar, A. T. Hsieh, R. Lin, S. L. Pentoney, D. L. Yang and A. P. Lee, *Lab Chip*, 2011, **11**, 3838–3845.
- 20 Y.-C. Tan, J. S. Fisher, A. I. Lee, V. Cristini and A. P. Lee, *Lab Chip*, 2004, **4**, 292–298.
- 21 Y. Bai, X. He, D. Liu, S. N. Patil, D. Bratton, A. Huebner, F. Hollfelder, C. Abell and W. T. S. Huck, *Lab Chip*, 2010, **10**, 1281–1285.
- 22 P. Abbyad, R. Dangla, A. Alexandrou and C. N. Baroud, *Lab on a Chip*, 2011, **11**, 813–821.
- 23 C. H. Schmitz, A. C. Rowat, S. Köster and D. A. Weitz, *Lab on a Chip*, 2009, **9**, 44–49.

- 24 A. Huebner, D. Bratton, G. Whyte, M. Yang, A. J. deMello, C. Abell and F. Hoffelder, *Lab on a Chip*, 2009, **9**, 692–698.
- 25 M. Sun, S. S. Bithi and S. A. Vanapalli, *Lab Chip*, 2011, **11**, 3949–3952.
- 26 W. Wang, C. Yang and C. M. Li, *Lab Chip*, 2009, **9**, 1504–1506.
- 27 X. Niu, F. Gielen, J. B. Edel and A. J. deMello, *Nat Chem*, 2011, **3**, 437442.
- 28 F. Sarrazin, L. Prat, N. Di Miceli, G. Cristobal, D. Link and D. Weitz, *Chemical engineering science*, 2007, **62**, 1042–1048.
- 29 H. Song, D. Chen and R. Ismagilov, *Angewandte chemie internationale edition*, 2006, **45**, 7336–7356.
- 30 H. Song, J. D. Tice and R. F. Ismagilov, *Angewandte Chemie International Edition*, 2003, **42**, 768–772.
- 31 T. A. Franke and A. Wixforth, *ChemPhysChem*, 2008, **9**, 2140–2156.
- 32 S.-Y. Teh, R. Lin, L.-H. Hung and A. P. Lee, *Lab Chip*, 2008, **8**, 198–220.
- 33 G. M. Whitesides, *Nature*, 2006, **442**, 368–373.
- 34 J. S. Eow and M. Ghadiri, *Colloids and Surfaces A: Physicochemical and Engineering Aspects*, 2003, **219**, 253 – 279.
- 35 J. S. Eow, M. Ghadiri, A. O. Sharif and T. J. Williams, *Chemical Engineering Journal*, 2001, **84**, 173 – 192.
- 36 J. S. Eow, M. Ghadiri and A. Sharif, *Colloids and Surfaces A: Physicochemical and Engineering Aspects*, 2003, **225**, 193 – 210.
- 37 P. Atten, L. Lundgaard and G. Berg, *Journal of Electrostatics*, 2006, **64**, 550 – 554.
- 38 L.-H. Hung, K. M. Choi, W.-Y. Tseng, Y.-C. Tan, K. J. Shea and A. P. Lee, *Lab Chip*, 2006, **6**, 174–178.
- 39 Y.-C. Tan, Y. Ho and A. Lee, *Microfluidics and Nanofluidics*, 2007, **3**, 495–499.
- 40 D. J. Collins, T. Alan, K. Helmerston and A. Neild, *Lab Chip*, 2013, **13**, 3225–3231.
- 41 P. Rogers and A. Neild, *Lab Chip*, 2011, **11**, 3710–3715.
- 42 K. Sriharan, C. J. Strobl, M. F. Schneider, A. Wixforth and Z. Guttenberg, *Applied Physics Letters*, 2006, **88**, –.
- 43 T.-D. Luong, V.-N. Phan and N.-T. Nguyen, *Microfluidics and Nanofluidics*, 2011, **10**, 619–625.
- 44 X. Ding, S.-C. S. Lin, M. I. Lapsley, S. Li, X. Guo, C. Y. Chan, I.-K. Chiang, L. Wang, J. P. McCoy and T. J. Huang, *Lab Chip*, 2012, **12**, 4228–4231.
- 45 D. J. Collins, T. Alan and A. Neild, *Lab Chip*, 2014, **14**, 1595–1603.
- 46 R. Walker, I. Gralinski, K. Keong Lay, T. Alan and A. Neild, *Applied Physics Letters*, 2012, **101**, –.
- 47 R. Shilton, M. K. Tan, L. Y. Yeo and J. R. Friend, *Journal of Applied Physics*, 2008, **104**, –.
- 48 C. Devendran, I. Gralinski and A. Neild, *Microfluidics and Nanofluidics*, 2014, 1–12.
- 49 P. Agrawal, P. S. Gandhi and A. Neild, *Journal of Applied Physics*, 2013, **114**, –.
- 50 P. Rogers, I. Gralinski, C. Galtry and A. Neild, *Microfluidics and Nanofluidics*, 2013, **14**, 469–477.
- 51 P. Augustsson, J. Persson, S. Ekstrom, M. Ohlin and T. Laurell, *Lab Chip*, 2009, **9**, 810–818.
- 52 G. Destgeer, K. H. Lee, J. H. Jung, A. Alazzam and H. J. Sung, *Lab Chip*, 2013, **13**, 4210–4216.
- 53 X. Ding, S.-C. S. Lin, B. Kiraly, H. Yue, S. Li, I.-K. Chiang, J. Shi, S. J. Benkovic and T. J. Huang, *Proceedings of the National Academy of Sciences*, 2012, **109**, 11105–11109.
- 54 J. Nam, Y. Lee and S. Shin, *Microfluidics and Nanofluidics*, 2011, **11**, 317–326.
- 55 J. Shi, X. Mao, D. Ahmed, A. Colletti and T. J. Huang, *Lab Chip*, 2008, **8**, 221–223.
- 56 J. Shi, D. Ahmed, X. Mao, S.-C. S. Lin, A. Lawit and T. J. Huang, *Lab Chip*, 2009, **9**, 2890–2895.
- 57 J. Shi, H. Huang, Z. Stratton, Y. Huang and T. J. Huang, *Lab Chip*, 2009, **9**, 3354–3359.
- 58 X. Ding, P. Li, S.-C. S. Lin, Z. S. Stratton, N. Nama, F. Guo, D. Slotcavage, X. Mao, J. Shi, F. Costanzo and T. J. Huang, *Lab Chip*, 2013, **13**, 3626–3649.
- 59 S.-C. S. Lin, X. Mao and T. J. Huang, *Lab Chip*, 2012, **12**, 2766–2770.
- 60 R. M. White and F. W. Voltmer, *Applied Physics Letters*, 1965, **7**, 314–316.
- 61 L. Rayleigh, *Proceedings of the London Mathematical Society*, 1885, **s1-17**, 4–11.
- 62 K. Yosioka, *Acustica*, 1955, **5**, 167–173.
- 63 L. P. Gor'kov, *Soviet Physics Doklady*, 1962, **6**, 773–775.
- 64 V. Skowronek, R. W. Rambach, L. Schmid, K. Haase and T. Franke, *Analytical Chemistry*, 2013, **85**, 9955–9959.
- 65 J. Lee and K. K. Shung, *The Journal of the Acoustical Society of America*, 2006, **120**, 1084–1094.
- 66 A. Ashkin, *Proceedings of the National Academy of Sciences*, 1997, **94**, 4853–4860.
- 67 D. G. Grier, *Nature*, 2003, **424**, 810–816.
- 68 J. Lee, K. Ha and K. K. Shung, *The Journal of the Acoustical Society of America*, 2005, **117**, 3273–3280.
- 69 J. Lee, C. Lee, H. H. Kim, A. Jakob, R. Lemor, S.-Y. Teh, A. Lee and K. K. Shung, *Biotechnology and Bioengineering*, 2011, **108**, 1643–1650.
- 70 J. Lee, S.-Y. Teh, A. Lee, H. H. Kim, C. Lee and K. K. Shung, *Applied Physics Letters*, 2009, **95**, year.
- 71 K. Svoboda and S. M. Block, *Annual review of biophysics and biomolecular structure*, 1994, **23**, 247–285.
- 72 J. Green, G. Kino and B. Khuri-Yakub, 1980 Ultrasonics Symposium, 1980, pp. 69–73.
- 73 M. K. Tan, J. R. Friend and L. Y. Yeo, *Phys. Rev. Lett.*, 2009, **103**, 024501.
- 74 L. Fisher, E. Mitchell and N. Parker, *Journal of Food Science*, 1985, **50**, 1201–1202.
- 75 K. Franke, M. Ross-Messemer, A. Menck, R. Hoeller, H. Schmidt and M. Weilmacht, *Ultrasonics, Ferroelectrics and Frequency Control, IEEE Transactions on*, 2003, **50**, 77–80.
- 76 L. L. Beranek, *Acoustics*, McGraw-Hill, New York, 1954.
- 77 P. Garstecki, M. J. Fuerstman, H. A. Stone and G. M. Whitesides, *Lab Chip*, 2006, **6**, 437–446.
- 78 W. Haberman and R. Sayre, *David Taylor Model Basin Reports*, 1958.